

Chandra Observation of a Group of Galaxies HCG 80: Does the Spiral-Only Group Have Hot Intragroup Gas?

Naomi Ota,¹ Umeyo Morita,² Tetsu Kitayama,³ and Takaya Ohashi²

¹*Cosmic Radiation Laboratory, RIKEN, 2-1 Hirosawa, Wako, Saitama 351-0198*

ota@crab.riken.jp

²*Department of Physics, Tokyo Metropolitan University, 1-1 Minami-Osawa, Hachioji, Tokyo 192-0397*

³*Department of Physics, Toho University, 2-2-1 Miyama, Funabashi, Chiba 274-8510*

(Received 2004 July 21; accepted 2004 August 22)

Abstract

We present an analysis of Chandra X-ray observations of a compact group of galaxies, HCG 80 ($z=0.03$). The system is a spiral-only group composed of four late-type galaxies, and has a high-velocity dispersion of 309 km s^{-1} . With high-sensitivity Chandra observations, we searched for diffuse X-ray emission from the intragroup medium (IGM); however, no significant emission was detected. We place a severe upper limit on the luminosity of the diffuse gas as $L_X < 6 \times 10^{40} \text{ erg s}^{-1}$. On the other hand, significant emission from three of the four members were detected. In particular, we discovered huge halo emission from HCG 80a that extends on a scale of $\sim 30 \text{ kpc}$ perpendicular to the galactic disk, whose X-ray temperature and luminosity were measured to be $\sim 0.6 \text{ keV}$ and $\sim 4 \times 10^{40} \text{ erg s}^{-1}$ in the 0.5–2 keV band, respectively. It is most likely to be an outflow powered by intense starburst activity. Based on the results, we discuss possible reasons for the absence of diffuse X-ray emission in the HCG 80 group, suggesting that the system is subject to galaxy interactions, and is possibly at an early stage of IGM evolution.

Key words: galaxies: clusters: individual (HCG 80) — galaxies: spiral — X-rays: galaxies — X-rays: ISM

1. Introduction

The majority of galaxies are found to reside in groups of galaxies (Tully 1987), and the intragroup medium may dominate the total baryon density of the local universe (Fukugita et al. 1998). Groups of galaxies should thus provide useful probes of structure formation in the universe, yet their physical nature is still highly unclear [see Hickson (1997) and Mulchaey (2000) for reviews]. The detection of extended X-ray emission has at least shown that a number of groups are gravitationally bound. The observed X-ray luminosities and the inferred gas mass, however, exhibit correlations with the gas temperature and galaxy velocity dispersion, much steeper than those predicted from a simple self-similar model (Mulchaey et al. 1996; Ponman et al. 1996). The X-ray emission also tends to be suppressed in spiral-dominated groups (Osmond, Ponman 2004), with a possible exception of HCG 57, from which Fukazawa et al. (2002) detected extended thermal X-ray emission with ASCA. Despite large observational errors, these facts are likely to indicate a close link between galaxy evolution and the properties of the intragroup medium.

Among the 109 galaxy groups observed with the ROSAT PSPC, extended X-ray emission has been detected in at least 61 groups. No diffuse emission was detected in 12 groups with only spiral members (Mulchaey et al. 2003). Recently the GEMS project constructed a large sample containing 60 groups based on the optical and ROSAT PSPC catalogues (Osmond, Ponman 2004).

The X-ray emission was detected for three of the five spiral-only groups; however, due to the limited quality of the data, the origin of the emission was not directly constrained, but was classified into hot halos of the individual galaxies based on their threshold in the spatial extent of $< 60 \text{ kpc}$. They suggested, based on the anti-correlation between the spiral fraction and the X-ray luminosity, that the presence of detectable hot diffuse gas is strongly related to the galaxy morphology. The possible absence of diffuse X-rays in the spiral-only groups would thus imply that either the bound group should contain at least one early-type galaxy, or the X-ray emission is preferentially suppressed in the spiral-only groups for some reason.

To further explore the nature of diffuse emission from the groups of galaxies, higher quality X-ray data are required. In particular, a high spatial resolution is crucial to separate the emission associated with individual galaxies from the diffuse component. Chandra and XMM-Newton are the most suitable satellites for this purpose, yet there have so far been few available observational results. Belsole et al. (2003) recently reported on the detection of diffuse X-ray emission from HCG 16 ($z = 0.013$) with the XMM-Newton EPIC cameras. The temperature and the luminosity were measured to be $0.49 \pm 0.17 \text{ keV}$ and $5.0 \times 10^{40} h_{70}^{-2} \text{ erg s}^{-1}$, respectively. The result obeys the $L_X - T$ relation obtained for brighter galaxy groups, though it is located at the extreme faint end, from which they suggested that HCG 16 is a bound system.

In this paper, we present a Chandra observation of a spiral-only group of galaxies, HCG 80. This group has

been one of the most plausible candidates, among the known spiral-only groups, for the positive detection of diffuse X-rays for the following reasons: (1) The high line-of-sight velocity dispersion of $\sigma_v = 309 \text{ km s}^{-1}$ implies a large gravitational potential; accordingly high X-ray luminosity and temperature of $L_X \sim 8.4 \times 10^{41} h_{70}^{-2} \text{ erg s}^{-1}$ and $kT \sim 0.8 \text{ keV}$ are expected from the $\sigma_v - L_X$ and $\sigma_v - T$ correlations (Ponman et al. 1996). The expected luminosity is close to the 3σ upper limit from the previous ROSAT PSPC, $L_X = 7.6 \times 10^{41} h_{70}^{-2} \text{ erg s}^{-1}$ (Ponman et al. 1996). (2) A compact galaxy distribution (4 members within $1'.7$ diameter) has led to a judgment that the HCG 80 galaxies are accordant members (Arp 1997; Sulentic 1997). (3) Two of the galaxies are classified as Im, which may indicate the galaxy-galaxy interaction in the group.

In addition, previous observations suggested a causal link between the starburst activity and the galaxy interactions [see Kennicutt (1998) for reviews]. Thus, a detailed spatial analysis of individual galaxies with an arc-second resolution of Chandra is a vital clue in constraining the connection between the outflowing gas and the intragroup medium without suffering from the contamination of point sources. The Chandra observations revealed X-ray views of the extended halo emission from the nearby starburst and normal galaxies in the dense environment. For example, the nature of diffuse X-ray emission from NGC 253 and NGC 55, both of which belong to the nearby spiral-only group, the Sculptor group, is considered separately in Strickland et al. (2002) and Oshima (2003). They exhibit observational evidence for galactic outflow from the spirals powered by star-formation activity. Strickland et al. (2004a, 2004b) studied ten star-forming disk galaxies with the Chandra X-ray and $H\alpha$ imaging data. From the correlations between a variety of X-ray quantities with multi-wavelength data, they quantitatively investigated supernova feedback on the galactic scale.

Through such detailed studies on spiral galaxies, we expect to obtain a new insight into the galaxy-IGM connection. Previous ROSAT observations showed that the groups of galaxies have a steeper luminosity-temperature relation compared to that of clusters of galaxies, which is noticeable for low temperature ($kT \lesssim 1 \text{ keV}$) systems. The preheating effect is suggested to be responsible for the steepening (e.g., Ponman et al. 1996); Helsdon and Ponman (2003) have proposed that spiral galaxies play a comparable role to early types in gas heating. However, it is still ambiguous; investigations are needed to clarify it further.

This paper is organized as follows. In the next section, we describe the Chandra observation of a galaxy group, HCG 80, and source detection in the field. In section 3, we present spatial and spectral analyses of HCG 80 member galaxies, and also constrain the diffuse X-ray emission from the hot intragroup gas. In section 4, we discuss the properties of the member galaxies and, in particular, the nature of the extended halo emission discovered in the brightest member of the group. We then discuss possible reasons for the absence of the strong X-ray emission from the intragroup gas of HCG 80.

Throughout this paper we adopt $\Omega_M = 0.3$, $\Omega_\Lambda = 0.7$; $h_{70} \equiv H_0 / (70 \text{ kms}^{-1} \text{ Mpc}^{-1}) = 1$; $1'$ corresponds to 36.1 kpc at $z = 0.0299$. The quoted errors indicate the 90% confidence range, unless otherwise stated. We use the solar abundance ratio of Anders and Grevesse (1989).

2. Observation and Source Detection

2.1. Chandra Observation of HCG 80

The group of galaxies HCG 80 consists of four late-type galaxies, HCG 80a-d, as shown in table 1 and figure 1. Their optical properties are also summarized in table 1. We observed HCG 80 with the Chandra Advanced CCD Imaging Spectrometer (ACIS-S) detector on 2003 August 18 (PI: N. Ota). The pointing coordinates were $15^{\text{h}}59^{\text{m}}12^{\text{s}}30$, $+65^{\circ}13'33''0$ (J2000), and the target was offset from the ACIS-S nominal aim point with a Y-offset of $-1'$. The CCD temperature was -120°C . The data reduction was performed using CIAO version 3.0.2 with CALDB version 2.25. We analyzed the light curve, and showed that there is no period of a high background level exceeding 3σ above the mean quiescent background rates. Thus, the net exposure time is 19712 s. We did not find any astrometry offset for the data. Since the data were taken with the VFaint mode, the particle background was reduced by screening out events with significant flux in border pixels of the 5×5 event islands.

2.2. Source Detection in the ACIS-S3 Field

We searched for X-ray sources in the ACIS-S3 field of view with the wadedetect algorithm with a significance parameter of 10^{-6} utilizing the 0.3–10 keV band image, and detected 20 in total, including HCG 80a and HCG 80b. We also found significant X-ray emission from the direction of HCG 80c. The counting rates of four member galaxies are summarized in table 2. In the following analysis, the detected point sources were excluded with a radius of 7-times the size of the Point Spread Function (PSF), which is defined as the 40% encircled energy radius at 1.5 keV at the source position.

The X-ray maximum positions of HCG 80a and b in the ACIS-S3 image are ($15^{\text{h}}59^{\text{m}}18^{\text{s}}9$, $+65^{\circ}13'57''3$) and ($15^{\text{h}}59^{\text{m}}21^{\text{s}}6$, $+65^{\circ}13'22''8$), respectively. Comparing these with the optical coordinates from Hickson, Kindl, and Auman (1989), they are consistent within $\lesssim 1''$. However, due to the limited photon statistics of the present X-ray data, there are uncertainties in the X-ray positions of the galaxies. We thus assumed the optical positions from Hickson, Kindl, and Auman (1989) as their centers in our analysis.

3. Analysis and Results

We analyze the X-ray emission from the individual galaxies in subsections 3.1, 3.2, and 3.3. In subsection 3.4 we exclude them from the group region and constrain the X-ray emission from the hot intragroup gas.

Table 1. Optical properties of member galaxies.

Object	Optical coords. (J2000)*		z	Diameters [†]	B [‡] [mag]	Type
	RA	Dec.				
HCG 80	15 ^h 59 ^m 12 ^s .4	+65°13′33″.3	0.02990			Group
HCG 80a	15 ^h 59 ^m 19 ^s .0	+65°13′57″.4	0.02994	50.8 × 10.8	15.66	Sd
HCG 80b	15 ^h 59 ^m 21 ^s .5	+65°13′22″.7	0.03197	20.4 × 17.4	16.37	Sa
HCG 80c	15 ^h 59 ^m 07 ^s .3	+65°14′00″.8	0.03186	19.6 × 16.4	16.06	Im
HCG 80d	15 ^h 59 ^m 12 ^s .1	+65°13′19″.3	0.03038	27.2 × 10.8	17.01	Im

* Optical coordinates of the object from Hickson, Kindl, and Auman (1989).

† Major axis [arcsec] × minor axis [arcsec].

‡ B magnitude.

Table 2. X-ray count rates, fluxes, and hardness ratios for member galaxies.

	R_{spec}^*	R_{max}^\dagger	Soft band		Hard band		HR^{**}
			S^\ddagger	$f_{X,S}^\S$	H^\parallel	$f_{X,H}^\#$	
HCG 80a	25	31	65.9 ± 6.4	3.4 ± 0.3	5.8 ± 3.5	0.7 ± 0.4	0.09 ± 0.05
HCG 80a, nucleus	–	2	14.7 ± 2.7	0.7 ± 0.1	3.5 ± 1.3	0.6 ± 0.2	0.24 ± 0.10
HCG 80a, disk+halo	–	31 – 2	50.3 ± 5.8	2.6 ± 0.3	2.9 (< 6.1)	0.3 (< 0.7)	0.06 ± 0.06
HCG 80b, nucleus	1.5	2	107.0 ± 7.4	5.3 ± 0.4	34.9 ± 4.2	6.2 ± 0.7	0.33 ± 0.05
HCG 80b, disk	–	10 – 2	6.2 ± 1.9	0.2 ± 0.1	0.4 (< 1.4)	0.04 (< 0.15)	0.06 (< 0.23)
HCG 80c	–	9.8	5.6 ± 1.9	0.2 ± 0.1	0.3 (< 1.3)	0.04 (< 0.15)	0.06 (< 0.24)
HCG 80d	–	13.6	1.7 (< 3.2)	0.06 (< 0.13)	< 2.7	< 0.05	1.6 ± 1.4

* The spectral extraction radius in arcsec (see subsection 3.3).

† The maximum radius in arcsec, used to estimate the counting rate, S and H , and the hardness ratio, HR .‡ The X-ray counting rate in the 0.5–2 keV band, S [10^{-4} counts s^{-1}].§ The X-ray flux in the 0.5–2 keV band, $f_{X,S}$ [10^{-14} ergs $^{-1}$ cm $^{-2}$].|| The X-ray counting rate in the 2–7 keV band, H [10^{-4} counts s^{-1}].# The X-ray flux in the 2–7 keV band, $f_{X,H}$ [10^{-14} ergs $^{-1}$ cm $^{-2}$].** The hardness ratio, $HR = H/S$.The quoted errors are the 1σ .

3.1. X-Ray Morphologies of Member Galaxies

As shown in table 2, because HCG 80a and b were detected with more than 10σ significance, we performed detailed analyses of the surface brightness distributions and energy spectra for those two galaxies. Since the significance of the X-ray emission from HCG 80c and d are low (2.6σ and $\lesssim 2\sigma$ in the soft band, respectively), we could only measure the fluxes (and luminosities under the assumptions of the spectral models). The results of flux estimations for the four member galaxies are also presented in table 2.

In order to constrain the spatial distribution of the X-ray emission from HCG 80a and b, we investigated the surface brightness distribution in two different ways: (1) a radial profile fitting and (2) a 1-dimensional profile fitting. In the former analysis, we compared the X-ray radial profile with the simulated PSF to constrain the emission from a nuclear source and the presence of diffuse emission. Since we found significant extended emission, particularly from HCG 80a, we studied the spatial distribution in detail in a latter analysis. We corrected the positional dependence of the telescope and the detector responses with exposure maps.

In the case of (1), we produced soft (0.5–2 keV) and hard (2–7 keV) band images and calculated the radi-

ally averaged surface brightness distributions centered at HCG 80a and b, as shown in figure 2. We fitted them separately with the PSF models, which were created by the HRMA PSF simulator, ChaRT, while specifying the locations of the sources and the spectral models derived from the spectral analysis (subsection 3.3). The PSF models were generated with sufficient photons so that the statistical uncertainty would be less than 10%, thus negligible compared to the Poisson error of the present data. We investigated the positional dependence of the background intensity using both the blank-sky data and the present data, to find that the background can be regarded as being constant within the statistical errors. The background intensities were then estimated from the $84'' < r < 160''$ ring region of the present pointing data to be $(4.73 \pm 0.20) \times 10^{-7}$ and $(5.31 \pm 0.21) \times 10^{-7}$ counts s^{-1} arcsec $^{-2}$ in the soft and hard bands, respectively (the errors are 1σ), and included as fixed constants in the fits.

HCG 80a

For HCG 80a, there is clearly an extended emission, particularly in the soft energy band compared with the PSF (figure 2a). We then evaluated the emission using the Gaussian functions to find that the single-component Gaussian model can not sufficiently fit the data, suggesting that at least two components are necessary to describe

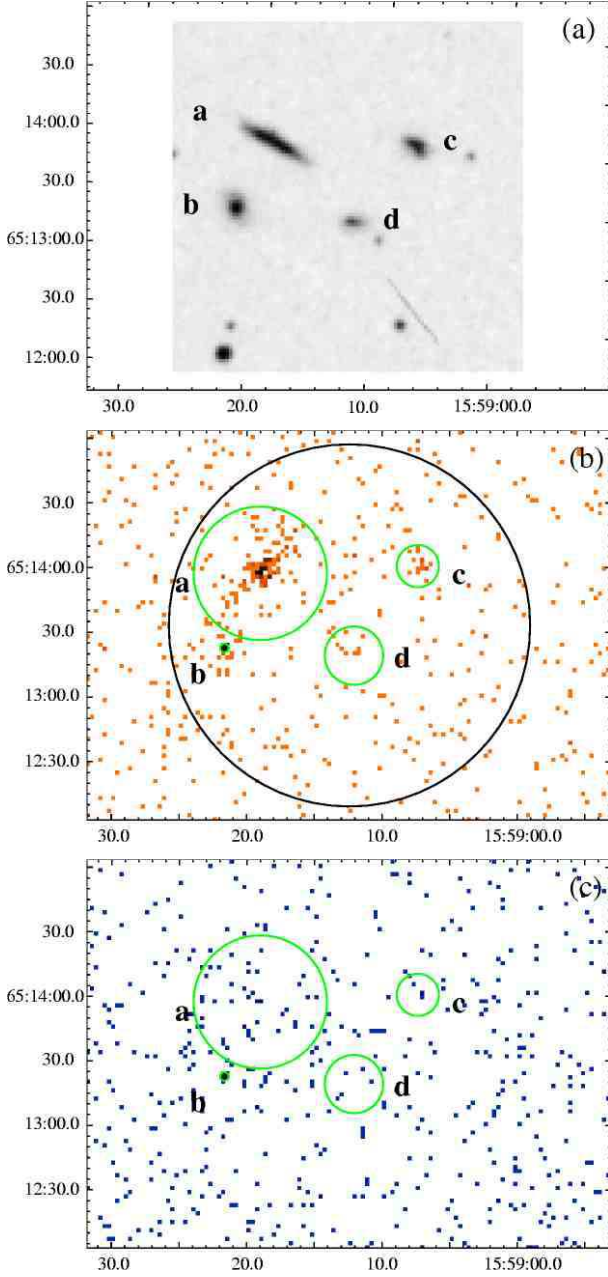


Fig. 1. Optical and X-ray images of the spiral-only group HCG 80. In the panel (a), the DSS image of the HCG 80 group is shown, where the four members are denoted by a–d. In panels (b) and (c), the Chandra X-ray images in the 0.5–2 keV and 2–7 keV bands are shown. The X-ray images are not smoothed, and are background inclusive. The image pixel size is $2'' \times 2''$. The member galaxies, HCG 80a–d, are indicated by green circles of radii $r = 31''$, $2''$, $9''$, and $13''$, respectively. In panel (b), the black color represents pixels with an X-ray surface brightness higher than 10 photons per image pixel. The group region used to constrain the diffuse emission in subsection 3.4 is shown with a circle of radius $84''$.

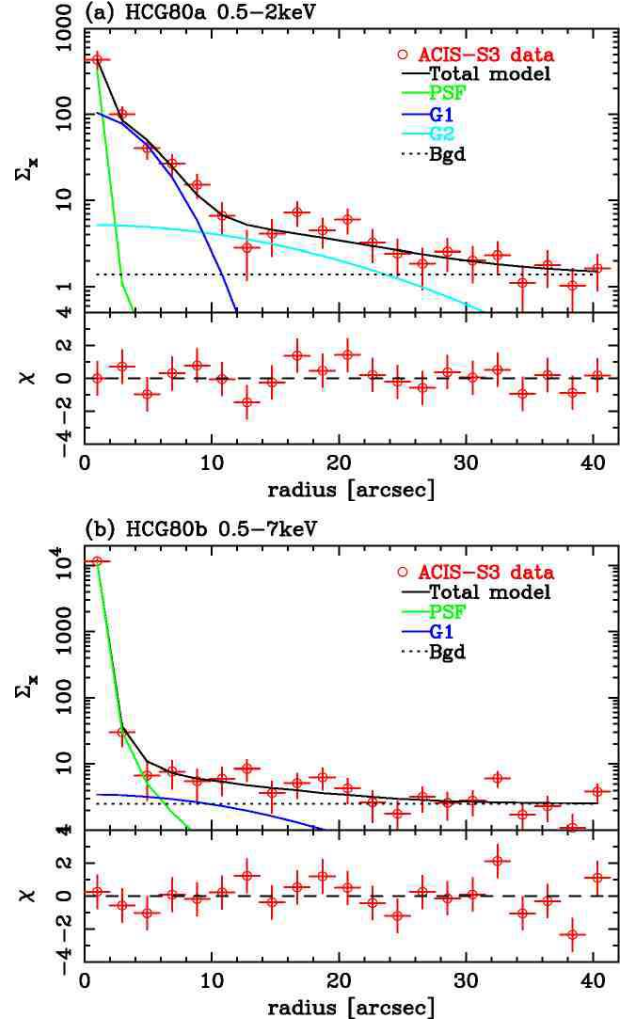


Fig. 2. Radial profile fitting for HCG 80a and b with the PSF and Gaussian(s) models. In panels (a) and (b), the ACIS-S3 radial surface brightness distribution for HCG 80a in the 0.5–2 keV and HCG 80b in the 0.5–7 keV are indicated by red crosses. The best-fit total model is shown with the black solid line in each panel, where the PSF and Gaussian components representing the disk and halo emissions are also indicated by the green, blue, and light-blue lines. The background intensity is indicated by the horizontal dotted line. In the upper panels Σ_X is in units of $10^{-9} \text{ photons s}^{-1} \text{ cm}^{-2} \text{ arcsec}^{-2}$, while in the bottom panels the residuals of the fits are shown in units of σ .

them. Thus, in figure 2a, we show the best-fit model consisting of the PSF and two Gaussians, where the diffuse emission is seen out to the maximum radius of $R_{\max} \sim 31''$ above the 2σ background level. We analyze the significance of the emission components and the properties in more detail later.

In the hard energy band, there is excess emission over the background within $2''$ from the HCG 80a optical center. The 2–7 keV counting rate is $(3.5 \pm 1.3) \times 10^{-4}$ counts s^{-1} . Under the current statistics, we could not constrain the spatial distribution. However, taking into account the spectral hardness inferred from the analysis in subsection 3.2 and the nuclear activity reported by Shimada et al. (2000), we suggest that the hard emission may be attributed to the central AGN in HCG 80a.

In the next step, we consider the soft diffuse emission from HCG 80a, based on a 1-dimensional profile fitting. Since the galaxy has a nearly edge-on inclination of $i = 86^\circ$, following Rubin et al. (1982) (see also Nishiura et al. 2000), the emission from the halo region is expected to be clearly resolved. From figure 1b, we find that the emission extends nearly along the perpendicular direction from the galactic disk of HCG 80a, whose position angle is 64° (Shimada et al. 2000). We thus extracted the 1D surface brightness profile along the minor axis of the galaxy, accumulated within $|r| < 24''$ of the major axis (figure 3a). The minor-axis profile was rebinned by a factor of 6; thus, each bin is $3''$. We carried out a χ^2 fitting with some simple models consisting of the Gaussian components for the diffuse emission and the PSF for the central emission, whose centers are fixed at the HCG 80a center position. As a result, neither the single Gaussian nor the PSF model could provide an acceptable fit; however, by adding another Gaussian component, the fit was significantly improved at the 95% level by the F-test. We show the results for the cases of Model 1 [equation (1)] and Model 2 [equation (2)] in table 3.

$$\Sigma_X = \Sigma_{\text{PSF}} + \Sigma_{\text{G1},0} e^{-(y-y_0)^2/\sigma_{\text{G1}}^2}, \quad (1)$$

$$\Sigma_X = \Sigma_{\text{G1},0} e^{-(y-y_0)^2/\sigma_{\text{G1}}^2} + \Sigma_{\text{G2},0} e^{-(y-y_0)^2/\sigma_{\text{G2}}^2}, \quad (2)$$

$$\Sigma_X = \Sigma_{\text{PSF}} + \Sigma_{\text{G1},0} e^{-(y-y_0)^2/\sigma_{\text{G1}}^2} + \Sigma_{\text{G2},0} e^{-(y-y_0)^2/\sigma_{\text{G2}}^2} + \Sigma_{\text{G3},0} e^{-(y-y_0)^2/\sigma_{\text{G3}}^2}, \quad (3)$$

where y_0 is fixed at the center of HCG 80a, and we assume $\sigma_{\text{G1}} < \sigma_{\text{G2}}$. We also fit the profile with Model 3 [equation (3)] and examine the significance of the emission from the central point source. Although the low photon statistics in the central emission resulted in no significant improvement over Model 2 in the F-test at the 95% confidence, we adopt Model 3 in the rest of our analysis regarding the presence of the optically identified AGN (Shimada et al. 2000) and the observed high hardness ratio in subsection 3.2.

From the fitting with Model 3, the width for the narrow Gaussian component was obtained to be $\sigma_{\text{G1}} = 3_{-1}^{+2}$ arcsec ($= 1.8_{-0.6}^{+1.2}$ kpc), which is very consistent with the optical scale of the galactic disk. The broad Gaussian component has a width of $\sigma_{\text{G2}} = 12_{-4}^{+8}$ arcsec ($= 7.2_{-2.4}^{+4.8}$ kpc), and thus largely extends compared to the disk scale. Accordingly,

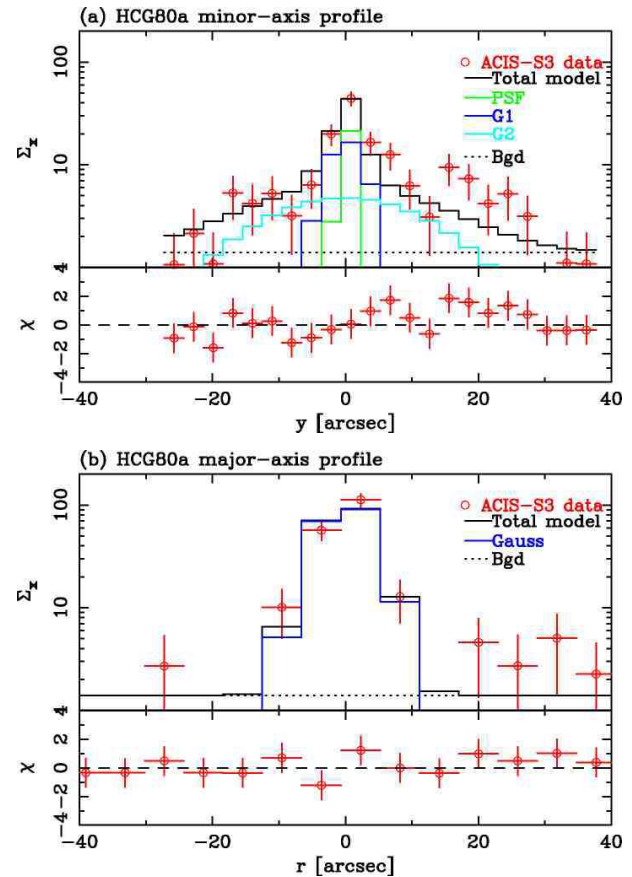


Fig. 3. Minor-axis and major-axis X-ray surface brightness distributions. In the panels (a) and (b), the crosses denote the observed 1-dimensional surface brightness profiles accumulated within $|r| < 24''$ of the major axis and $|y| < 5''$ of the minor axis in the soft band, respectively. The surface brightness, Σ_X , is in units of 10^{-9} photons $s^{-1} \text{cm}^{-2} \text{arcsec}^{-2}$. In the panel (a), the solid black line shows the result of the fitting with Model 3. The PSF, narrow Gaussian, broad Gaussian, and background components are indicated by the green, blue, light-blue, and dotted black lines, respectively. In the panel (b), the solid black, blue, and dotted lines show the best-fit total model, Gaussian and the background components, respectively.

we refer to the narrow and broad Gaussian components, respectively, as the “disk” and “halo” components hereafter. The extent of the halo emission detected above the 2σ background level is $-26'' < y < 26''$, corresponding to 31.2 kpc in total. The origin of this huge X-ray halo is discussed in section 4.

We estimated the luminosity of each component assuming the MEKAL model with an average temperature of 0.56 keV for the disk and the halo, and a power-law model with $\Gamma = 2.0$ for the nucleus. Here, the same definitions as those of Strickland et al. (2004a) are used to define the emission regions for the nuclear (N), disk (D), and halo (H) components. Namely the luminosities ($L_{X,N}$, $L_{X,D}$, and $L_{X,H}$) are accumulated from the $r < 1$ kpc circle, a rectangular aperture oriented along the minor axis of major-axis length 28.9 kpc and extending between $-2 \text{ kpc} < y < 2 \text{ kpc}$, and a $28.9 \text{ kpc} \times 39.1 \text{ kpc}$ rectangular aperture oriented

Table 3. Results of the 1D fitting for HCG 80a in the soft band.

Parameter	Model 1 PSF+G1	Model 2 G1+G2	Model 3 PSF+G1+G2
PSF [photons s ⁻¹ cm ⁻²]	43 ⁺¹³ ₋₁₄ × 10 ⁻⁹	–	25(< 45) × 10 ⁻⁹
Σ _{G1,0} [photons s ⁻¹ cm ⁻² arcsec ⁻²]	7.6 ^{+5.2} _{-2.8} × 10 ⁻⁹	36.4 ^{+19.5} _{-12.6} × 10 ⁻⁹	17.2 ^{+31.7} _{-12.4} × 10 ⁻⁹
σ _{G1} [arcsec]	10 ± 4	2 ± 1	3 ⁺² ₋₁
Σ _{G2,0} [photons s ⁻¹ cm ⁻² arcsec ⁻²]	–	5.6 ^{+3.8} _{-2.8} × 10 ⁻⁹	4.7 ^{+3.5} _{-2.8} × 10 ⁻⁹
σ _{G2} [arcsec]	–	12 ⁺⁶ ₋₄	12 ⁺⁸ ₋₄
χ ² /dof	26.2/19	22.7/18	20.6/17

along the minor axis with excluding the N and D regions. We obtained $L_{X,D} = 2.2 \times 10^{40}$ erg s⁻¹, $L_{X,H} = 3.8 \times 10^{40}$ erg s⁻¹, and $L_{X,N} = 1.7 \times 10^{40}$ erg s⁻¹ in the 0.5–2 keV, respectively. The results are also given in table 5.

We also notice that the intensity of the halo emission from the Northern hemisphere is stronger than that of the Southern by a factor of $\sim 2.7 \pm 2.1$ if we fit the Northern and Southern halos separately with Model 3 while fixing the model parameters, except for $\Sigma_{G2,0}$ at the best-fit values derived in the above analysis. Thus, there may be some asymmetry. However, because the current statistics is limited, we could not further constrain the spatial distribution of the halo emission.

We show the major-axis profile accumulated within $|y| < 5''$ of the minor axis in figure 3b. It could be fitted by a Gaussian with $\sigma = 4 \pm 1$ arcsec ($= 2.4 \pm 0.6$ kpc) and a normalization for the central surface brightness of $108^{+49}_{-27} \times 10^{-9}$ photons s⁻¹cm⁻²arcsec⁻². We found that the width is close to that of the narrow component in Model 3, namely $\sigma \sim \sigma_{G1}$. Thus, the disk emission is concentrated within about $3''.5$ from the center, while we did not find significant emission extending over the optical scale of the galactic disk.

HCG 80b

From a comparison to the simulated PSFs, we found that the innermost data points of the radial surface brightness distributions are well consistent with the PSFs in both the soft and hard energy bands, and resultant χ^2 values of 24.6 and 34.4 for 20 degrees of freedom. However, we found that there are systematic residuals over the PSFs in several consecutive bins around $r \sim 10''$, which can be attributed to the extra emission around the point source. Because the emission is found within a radius roughly corresponding to the size of the optical disk, $\sim 10''$, we refer to it as the disk component, while referring to the central point source as the nucleus component hereafter. The photon counts coming from the disk component in a radius range of $2'' < r < 10''$ are 12 ± 4 and < 3 , in the soft and hard bands, respectively (see also table 2).

In order to further constrain the emission profile, we attempted to fit the 0.5–7 keV radial profile with the PSF plus Gaussian model, as shown in figure 2. This provided an acceptable fit with $\chi^2/\text{dof} = 19.3/18$, and the PSF intensity was obtained as $(1.13 \pm 0.17) \times 10^{-5}$ photons s⁻¹cm⁻²; the Gaussian normalization and the width are $3.5^{+3.5}_{-2.6} \times 10^{-9}$ photons s⁻¹cm⁻²arcsec⁻²

and 12^{+7}_{-5} arcsec ($= 7^{+4}_{-3}$ kpc), respectively. Because the model parameters are associated with large uncertainties, the emission profile, particularly for the diffuse emission, is not well constrained, which we consider as being due to the low signal-to-noise ratios at the outer radius. We therefore decide to fix the maximum radius at the size of the optical disk, $R_{\text{max}} = 10''$, when evaluating the X-ray intensities for the disk emission. Within $2''$ from the HCG 80b peak, the central nuclear component dominates the total emission, and we use the maximum radius of $R_{\text{max}} = 2''$ for the HCG 80b nucleus. The luminosities of the nucleus ($r < 2''$) and the disk ($2'' < r < 10''$) were estimated to be $(2.9 \pm 0.2) \times 10^{41}$ erg s⁻¹ and $(5.8 \pm 1.8) \times 10^{39}$ erg s⁻¹ in the 0.5–7 keV band assuming a power-law model with $\Gamma = 1.9$ (see subsection 3.3) and the MEKAL model with $kT = 0.5$ keV and $Z = 0.1$ solar, respectively.

3.2. Hardness Ratio Analysis

To provide a quantitative evaluation of the spatial variation of the X-ray spectra, the hardness ratios for the central and the surrounding disk (+ halo) regions are given in table 2. We define the hardness ratio as $HR \equiv H/S$, where S and H are the photon counts in the 0.5–2 and 2–7 keV bands, respectively. Due to the low significance of the emission from HCG 80c and d, we give the values derived for the entire galaxy regions for these two galaxies. There is an indication that the HCG 80a central emission ($r < 2''$) is hard compared with the outer ($2'' < r < 31''$) region. If we simply assume the spectra as being described by a power-law (or the $Z = 0.1$ solar MEKAL) model attenuated by Galactic absorption, the power-law indices (or the gas temperature) for the nucleus and the disk + halo regions of HCG 80a correspond to $\Gamma = 2.2 \pm 0.4$ ($kT = 2.6 \pm 1.4$ keV) and $\Gamma = 3.5 (> 2.8)$ ($kT = 1.0 (< 1.4)$ keV), respectively. While the HCG 80b nucleus region ($r < 2''$) shows a large HR value, corresponding to a power-law index of 1.9 ± 0.2 , the HR for the outer disk region ($2'' < r < 10''$) was not constrained. In the next subsection we explore the spectra from the HCG 80a “nucleus + disk + halo” and the HCG 80b “nucleus” regions based on thermal and/or non-thermal spectral modeling to constrain their origins.

Strickland et al. (2004a) suggested, based on the Chandra data for ten star-forming galaxies, that the disk emission tends to be harder than the halo emission; however, we did not find any meaningful HR variation between

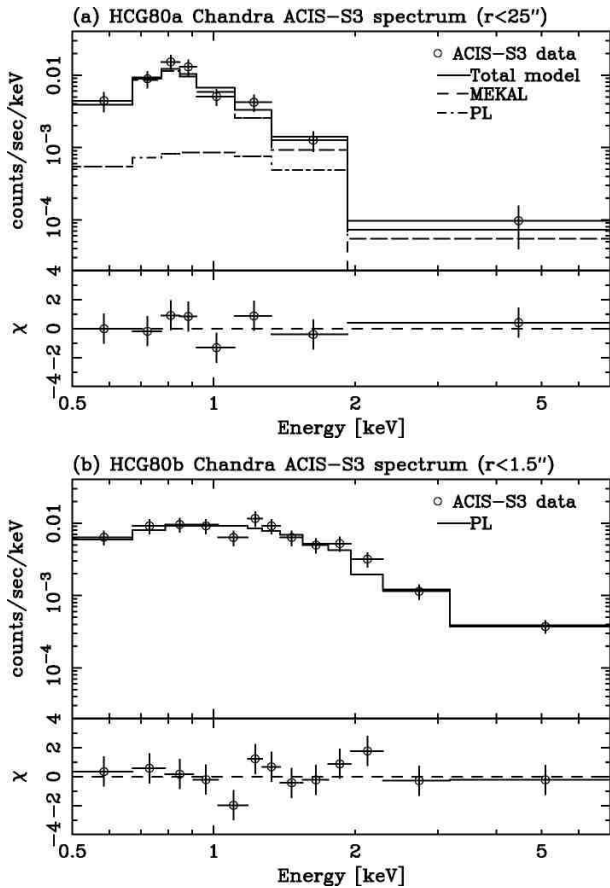


Fig. 4. Chandra ACIS-S3 spectra of HCG 80a (a) and HCG 80b (b). In the upper panels, the open circles denote the observed spectra and the step functions show the best-fit spectral models (the MEKAL+Power-law model for HCG 80a and the Power-law model for HCG 80b) convolved with the telescope and the detector response functions. In the lower panels, the residuals of the fit are shown.

the two regions in HCG 80a due to the poor photon statistics of the present data.

3.3. X-Ray Spectra of Member Galaxies

We extracted X-ray spectra for HCG 80a and b from circular regions with radii $R_{\text{spec}} = 25''$ and $1.''5$, respectively (figure 4). Note that R_{spec} was so chosen that about 90% of the X-ray photons from each galaxy could be accumulated and that two galaxies might not overlap each other. We fitted the spectra with the power-law model and the MEKAL thin-thermal plasma model (Mewe et al. 1985, 1986; Kaastra 1992; Liedahl et al. 1995). The absorption column density was fixed at the Galactic value, $N_{\text{H}} = 2.5 \times 10^{20} \text{ cm}^{-2}$ (Dickey, Lockman 1990).

HCG 80a

For HCG 80a, the power-law spectral model was rejected at the 99% confidence level. On the other hand, the MEKAL model provided a good fit to the data with a χ^2 value of 5.9 for 5 degrees of freedom. We obtained the temperature and the metallicity to be $0.59^{+0.12}_{-0.10} \text{ keV}$

and $0.07^{+0.18}_{-0.05}$ solar, respectively. Though the AGN emission was estimated to be only $\sim 20\%$ of the total emission from the image analysis, we checked whether the temperature determination of the intragroup gas was influenced by the AGN component in the following two ways: (1) excluded the central $r < 5''$ circular region from the HCG 80a overall spectrum, and fit it with the MEKAL model, and (2) fit the overall spectrum with the two-component model, where the power-law index and the metallicity were, respectively, fixed at 2.0 and 0.1 solar. We found that both of the analyses yielded consistent temperatures ($\sim 0.6 \text{ keV}$) within the errors. We give the results for case (2) in table 4. We also confirmed that the ratio of the X-ray luminosities between the AGN and the diffuse components is consistent with the result of the image analysis under Model 3 within 10%.

HCG 80b

We found that the HCG 80b spectrum can be fitted either by the power-law model or the MEKAL model. Even though the MEKAL temperature of $kT \sim 3.5 \text{ keV}$ may be consistent with a collection of Low Mass X-ray Binaries, the observed luminosity of $2.6 \times 10^{41} \text{ erg s}^{-1}$ is by more than 3 orders higher than the values for normal spiral galaxies. On the other hand, the power-law index of $\Gamma = 1.94^{+0.19}_{-0.18}$, deduced from the X-ray spectral fitting is consistent with the values of known AGNs. We also estimated the α_{OX} index, which is the slope of a hypothetical power law connecting the B band and 2 keV, to be 1.9. The value is larger compared with the result of the ROSAT large quasar survey, but within the scatter of the quasars (figure 2 of Green et al. 1995). Thus, the emission from the central $r < 1.''5$ region is most likely to originate from the AGN in the galaxy.

3.4. Constraints on the Hot Diffuse Emission

In order to constrain the X-ray emission from the hot intragroup medium, we defined the group region with a $r = 84'' = 50.5 \text{ kpc}$ circle, whose center is the same as that of HCG 80, $15^{\text{h}}59^{\text{m}}12^{\text{s}}.4$, $+65^{\circ}13'33''.3$ (Hickson et al. 1989), which encompasses the optical disks of the four member galaxies (figure 1b). We subtracted the background and the galaxy contributions from the total photon counts in the group region and derived the intensity of the intragroup emission. Note that we used the background intensity estimated from the outer-ring region. The source counts within $31''$ from the brightest member, HCG 80a, were estimated based on the results of the image analysis presented in subsection 3.1, while for HCG 80b–d, the observed source counts within circles of radii $R_{\text{max}} = 10''$, $9.''8$ and $13.''6$, approximately equal to the sizes of the optical disks, were used.

Subtracting the galaxy contributions, 130 ± 12 , 223 ± 15 , 11 ± 3 , $3 (< 5)$ counts for HCG 80a–d and the background, 213 ± 9 counts from the total photon counts of 576 ± 24 in the group region, we found that there is no significant emission from the hot IGM, and that the 3σ upper limit is obtained to be 92 photons in the 0.5–2 keV band. We also confirmed that the present estimation of the IGM

Table 4. Results of spectral fittings for HCG 80a and HCG 80b.

Galaxy	Model	Parameter	Value (90% error)	χ^2/dof	
HCG 80a ($R_{\text{spec}} = 25''$)	MEKAL	kT [keV]	$0.59^{+0.12}_{-0.10}$	5.9/5	
		Z [solar]	$0.07^{+0.18}_{-0.05}$		
		z	0.02994 (F)		
		k_M^*	$9.9^{+8.3}_{-5.7} \times 10^{-5}$		
		Γ	2.0 (F)		
	PL +MEKAL	PL	k_P^\dagger	$< 5.2 \times 10^{-6}$	4.4/5
			kT [keV]	$0.56^{+0.12}_{-0.17}$	
			Z [solar]	0.1 (F)	
			z	0.02994 (F)	
			k_M^*	$7.4^{+2.9}_{-1.9} \times 10^{-5}$	
			$f_{X,P}$ [erg s $^{-1}$ cm $^{-2}$] ‡	$< 2.1 \times 10^{-14}$	
			$L_{X,P}$ [erg s $^{-1}$] ‡	$< 4.6 \times 10^{40}$	
			$L_{\text{bol},P}$ [erg s $^{-1}$] ‡	$< 6.1 \times 10^{40}$	
			$f_{X,M}$ [erg s $^{-1}$ cm $^{-2}$] §	$(2.8 \pm 0.5) \times 10^{-14}$	
			$L_{X,M}$ [erg s $^{-1}$] §	$6.5^{+0.8}_{-1.2} \times 10^{40}$	
$L_{\text{bol},M}$ [erg s $^{-1}$] §	$7.8^{+1.2}_{-1.6} \times 10^{40}$				
HCG 80b ($R_{\text{spec}} = 1''5$)	PL	Γ	$1.94^{+0.19}_{-0.18}$	10.7/11	
		k_P^\dagger	$2.5^{+0.3}_{-0.3} \times 10^{-5}$		
		$f_{X,P}$ [erg s $^{-1}$ cm $^{-2}$] ‡	$10.6^{+1.6}_{-1.8} \times 10^{-14}$		
		$L_{X,P}$ [erg s $^{-1}$] ‡	$(2.6 \pm 0.3) \times 10^{41}$		
		$L_{\text{bol},P}$ [erg s $^{-1}$] ‡	$(3.5 \pm 0.4) \times 10^{41}$		
	MEKAL	MEKAL	kT [keV]	$3.5^{+1.6}_{-1.0}$	12.7/10
			Z [solar]	< 0.17	
			z	0.03197 (F)	
			k_M^*	$1.07^{+0.16}_{-0.14} \times 10^{-4}$	

* Normalization factor for the MEKAL model, $k_M = \int n_e n_H dV / 4\pi (D_A (1+z))^2 [10^{-14} \text{ cm}^{-5}]$, where D_A is the angular diameter distance to the source.

† Normalization factor for the power-law (PL) model, k_P [photons keV $^{-1}$ cm $^{-2}$ s $^{-1}$] at 1 keV.

(F) Fixed parameters.

‡ The 0.5–7 keV X-ray flux and the 0.5–7 keV luminosity for the PL model.

§ The 0.5–7 keV X-ray flux and the 0.5–7 keV luminosity for the MEKAL model.

emission is not affected by the choice of the extraction radii, R_{max} for the galaxies b–d; if we change R_{max} by a factor of 0.5–1.5, the result changes by only $\lesssim 10\%$. If we further assume the temperature and the metallicity of the gas to be comparable to those derived for HCG 16, $kT \sim 0.5$ keV and $Z \sim 0.1$ solar (Belsole et al. 2003), the bolometric luminosity is constrained as $L_X < 6.3 \times 10^{40}$ erg s $^{-1}$ (3σ). We show the location of HCG 80 on the $L_X - f_{\text{spiral}}$ plane in figure 5.

4. Discussion

From a high-resolution Chandra observation of the spiral-only group HCG 80, we detected significant X-ray emission from three of the four member galaxies (HCG 80a, b, and c), and investigated the spatial distribution and the spectral features for HCG 80a and b in detail. In particular, we discovered halo emission from HCG 80a, which extends to ~ 30 kpc perpendicular to the galactic disk. We compare the X-ray luminosity of the member galaxies to those of the optical in subsection 4.1, and further discuss the origin of the halo emission from HCG 80a in subsection 4.2. On the other hand, we found

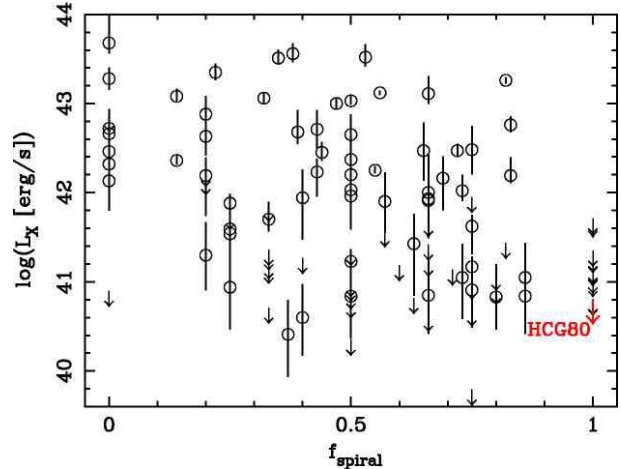


Fig. 5. $L_X - f_{\text{spiral}}$ relation. The groups with constrained/unconstrained bolometric luminosity from the ROSAT PSPC survey (Mulchaey et al. 2003) are plotted with open circle/arrow, as a function of the spiral fraction. The upper limit on the bolometric luminosity for the hot diffuse gas in HCG 80, obtained from the present Chandra analysis, is indicated by the red arrow.

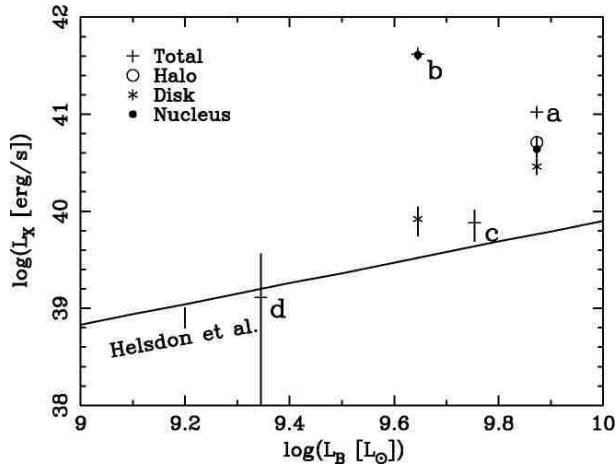


Fig. 6. $L_X - L_B$ relation. The bolometric luminosity of the overall galaxy region is plotted against the B luminosity [L_\odot] for each galaxy (cross). For HCG 80a, the nucleus, disk and halo components are also separately indicated by the solid circle, asterisk, and open circle, respectively. For HCG 80b, the nucleus and the disk components are indicated by the solid circle and asterisk, respectively. The error bars are the 1σ . The solid line represents the best-fit $L_X - L_B$ relation for the late-type group galaxies (Helsdon et al. 2001).

that there is no significant emission from the group region. The absence of strong X-ray emission is discussed in subsection 4.3.

4.1. X-Ray Properties of the Member Galaxies

We show the relation between the bolometric X-ray luminosity, L_X , and the B band luminosity, L_B , for the HCG 80 members in figure 6. In addition to the overall luminosities of the galaxies, the luminosities of the nucleus, disk, and halo regions are separately plotted for HCG 80a and b. The X-ray luminosities were estimated from the spectral analyses for HCG 80a and the HCG 80b nucleus. However, because the spectra for the HCG 80b disk, HCG 80c and d were not constrained, we assume the thermal emission with $kT = 0.5$ keV and $Z = 0.1$ solar to convert the photon counting rates in the soft band (table 2) to L_X . This assumption may be valid because the hardness ratios listed in table 2 are in agreement with the values for soft thermal emission.

Comparing with the best-fit $L_X - L_B$ relation for the late-type galaxies in the Helsdon et al. (2001) sample, we found that the disk component of HCG 80b and the overall luminosities of HCG 80c and d are consistent with their relation if we take into account the measurement errors and the large data scatter among the other late-type galaxies. On the other hand, HCG 80a and b clearly show a higher L_X value than expected from the $L_X - L_B$ relation from Helsdon et al. (2001). They noted that the galaxies associated with the AGN and/or the starburst activities tend to lie above the best-fitting line, namely they have enhanced X-ray emission relative to the optical band. Thus considering from the thermal nature of the extended emission of HCG 80a and the hard spectrum of the point-like emission

from HCG 80b found in the previous section, the higher L_X values agree with their indication.

Furthermore, starburst galaxies are often identified based on their high IR luminosity and warm FIR colors, $f_{60}/f_{100} > 0.4$. The FIR fluxes are available only for HCG 80a. From the IRAS 12-, 25-, 60-, and 100- μm fluxes, $(f_{12}, f_{25}, f_{60}, f_{100}) = (0.10, 0.16, 2.31, 5.16)$ Jy, the IR luminosity is $L_{IR} = 12.3 \times 10^{10} L_\odot$ utilizing $L_{IR} = 5.67 \times 10^5 D_{\text{Mpc}}^2 (13.48 f_{12} + 5.16 f_{25} + 2.58 f_{60} + f_{100}) L_\odot$ (Sanders, Mirabel 1996). This is consistent with the $L_X - L_{IR}$ correlation for starburst galaxies (Strickland et al. 2004b; Helsdon et al. 2001). $f_{60}/f_{100} = 0.45$; hence HCG 80a is ‘‘FIR warm’’. Thus, the above facts strongly support that the X-ray emission from HCG 80a is produced by starburst activity. In the next subsection, we derive some physical parameters to characterize a starburst, and compare them to the previous measurements on other starburst galaxies, in light of energy feedback from massive stars.

4.2. Starburst Activity in HCG 80a

The huge extraplanar emission discovered in HCG 80a reminds us of the bipolar outflow in a bright starburst galaxy, such as M 82 (e.g., Lehnert et al. 1999). The X-ray luminosity from the HCG 80a halo is determined to be $\sim 4 \times 10^{40}$ erg s $^{-1}$ (table 5), which is even larger than that reported for bright starburst galaxies. We show a detailed comparison of the luminosities derived in subsection 3.1 and the emission-weighted X-ray temperature to the values reported for M 82 and NGC 253 (Strickland et al. 2004a). We also show the star-formation rate estimated from the IR luminosity, $\text{SFR}_{IR} = 21.1 M_\odot \text{yr}^{-1}$, where $\text{SFR}_{IR} = 4.5 \times 10^{-44} L_{IR}$ [erg s $^{-1}$] (Kennicutt 1998).

In order to investigate the physical properties of the X-ray emitting thermal plasma in the halo, we treated the emission region as a cylinder of diameter 4 kpc and height 30 kpc, and estimated the electron density and the gas mass. Thus, the following values are meaningful only as order-of-magnitude estimates. The volume of the cylinder is $V = 1.1 \times 10^{67}$ cm 3 and the emission integral of the corresponding region is $EI = n_e n_H V = 1.44 \times 10^{64}$ cm $^{-3}$ based on the result of the spectral fitting. These yielded the electron density, the thermal pressure, the thermal energy, and the gas mass for an average temperature of $T = 6.5 \times 10^6$ K, as follows:

$$n_e = 4.0 \times 10^{-2} \text{ cm}^{-3}, \quad (4)$$

$$P_{\text{th}}/k = n_e T = 2.6 \times 10^5 \text{ K cm}^{-3}, \quad (5)$$

$$M_{\text{gas}} = \mu_e m_p n_e V = 4.3 \times 10^8 M_\odot, \quad (6)$$

$$E_{\text{th}} = \frac{3}{2} (n_e + n_H) k T V = 1.1 \times 10^{57} \text{ erg}, \quad (7)$$

where we adopt $n_H = (\mu_e/\mu_H)n_e$, $\mu_e = 1.167$, and $\mu_H = 1.40$. The above values are higher by about a factor of $\gtrsim 5$ than those obtained for NGC 253 (Strickland et al. 2002) if we neglect any systematic error.

The radiative cooling timescale of the gas and the mass-cooling rate are estimated to be $t_{\text{cool}} \sim E_{\text{th}}/L_{\text{bol}} = 390$ Myr and $\dot{M}_{\text{gas}} \sim 1.1 M_\odot \text{yr}^{-1}$. Then, supposing that the flow

Table 5. Halo, disk, nuclear, and total luminosities.

Galaxy	$\langle kT \rangle^*$	Band [†]	$L_{X,H}^{\ddagger}$	$L_{X,D}^{\S}$	$L_{X,N}^{\parallel}$	$L_{X,tot}^{\#}$	L_B^{**}	L_{IR}^{**}	$SFR_{IR}^{\dagger\dagger}$
HCG 80a	$0.56^{+0.12}_{-0.17}$	0.5–2	3.5 ± 0.5	2.0 ± 0.4	1.6 ± 0.3	7.1 ± 0.7	0.75	12.3	21.1
HCG 80a	$0.56^{+0.12}_{-0.17}$	0.3–2	4.5 ± 0.7	2.6 ± 0.4	2.1 ± 0.4	9.2 ± 0.9	0.75	12.3	21.1
M 82 ^{‡‡}	0.37	0.3–2	0.41	1.6	2.3	4.3	0.33	5.36	9.2
NGC 253 ^{‡‡}	0.25	0.3–2	0.12	0.33	0.094	0.55	0.58	2.10	3.6

* Emission-weighted X-ray temperature of the diffuse emission in keV.

† Energy band in keV used to calculate the X-ray luminosities.

‡, §, ∥ X-ray luminosities for the halo (H), the disk (D), and the nucleus (N) regions in $10^{40} \text{ erg s}^{-1}$.

Total X-ray luminosity for the H + D + N regions in $10^{40} \text{ erg s}^{-1}$. The errors of the luminosity measurements for HCG 80a are the 1σ .

** B and IR luminosities in $10^{10} L_{\odot}$.

†† Star-formation rate from the IR luminosity, $SFR_{IR} = 4.5 \times 10^{-44} L_{IR} [\text{erg s}^{-1}]$ (Kennicutt 1998).

‡‡ The values were taken from Strickland et al. (2004a).

velocity may be approximated by the sound speed of the gas, $v_{\text{flow}} \sim v_s = 292 \text{ km s}^{-1}$, the time necessary to travel the distance of 15 kpc (a half of the height of the cylinder) is $t_{\text{flow}} \sim 50 \text{ Myr}$. Since $t_{\text{cool}} \gg t_{\text{flow}}$, the condition for maintaining halo emission seems to be satisfied.

The above calculations and the high SF rate inferred from the IR luminosity indicate that an enormous thermal energy of $\sim 10^{57} \text{ erg}$ would be supplied through successive SN explosions and the formation of superbubbles. We will estimate the SN rate and also compare the estimated quantities with the “disk blowout” condition to test the plausibility of the present interpretation.

Assuming a Type II supernova energy input of 10^{51} erg and a canonical value for the thermalization efficiency of 10%, the thermal energy contained in the hot gas requires $\sim 10^7 \text{ SNe}$. Thus, the SN rate is expected to be $\sim 10^7/t_{\text{flow}} = 0.2 \text{ yr}^{-1}$ to keep the $\sim 10^7$ ejecta in the halo region. Alternatively, with the IR luminosity and the relation from Heckman, Armus, and Miley (1990), the SN rate is $R_{\text{SN}} = 0.2 L_{\text{IR}}/10^{11} L_{\odot} \sim 0.25 \text{ yr}^{-1}$. Then, if the successive star formation had lasted in the past for $t_{\text{SF}} = 40 \text{ Myr}$, and one supernova may supply thermal energy of $10^{50} \text{ erg s}^{-1}$, the SN rate of 0.25 yr^{-1} can account for the thermal energy in the halo of $E_{\text{th}} \sim 10^{57} \text{ ergs}$ [equation (7)]. The duration of $t_{\text{SF}} = 40 \text{ Myr}$ is comparable to the timescale of the outflow, t_{flow} , and seems also to be reasonable from the point of view of the typical lifetime of massive stars, $\sim 10 \text{ Myr}$.

We next consider whether the gas can really escape from the galaxy potential well against the gravitational force. The escape velocity was estimated to be $v_{\text{esc}} \sim 120 \text{ km s}^{-1}$ (or equivalently $kT \sim 0.14 \text{ keV}$) utilizing a mass-to-light ratio of $M/L_B \simeq 60h(R/0.1\text{Mpc})M_{\odot}/L_{\odot}$ for spiral galaxies (Bahcall et al. 1995). Here, we assumed that the galaxy mass within R is given by $M \sim Rv_{\text{esc}}^2/G$, and adopted $R = 15 \text{ kpc}$, which corresponds to the isophotal radius, R_{25} (Hickson 1993). Note that the rotation curve was measured within the central $r \lesssim 4 \text{ kpc}$ by Nishiura et al. (2000). Though it is difficult to infer v_{esc} from their result, due to the existence of asymmetry between the approaching and receding sides of the galaxy, the average rotation velocity is roughly $\sim 130 \text{ km s}^{-1}$, and thus comparable to the value estimated above. Therefore, the observed temperature of 0.6 keV is sufficiently high for

the gas to escape into intergalactic space.

The critical mechanical luminosity for the disk blowout [see Strickland et al. (2004b) and references therein] is calculated as $L_{\text{crit}} = 4.2 \times 10^{40} \text{ erg s}^{-1}$. The mechanical energy injection of the halo may be given by $L_W \sim L_{X,H} = 3.5 \times 10^{40} \text{ erg s}^{-1}$. Therefore, $L_W \sim L_{\text{crit}}$. Furthermore, we compare the density of the halo region derived in equation (4) to a model calculation of a disk-halo interaction by Norman and Ikeuchi (1989) to find that it is within the chimney/starburst phase where the blow-out occurs.

The mass-flow rate is estimated to be $\dot{M}_{\text{flow}} \sim M_{\text{gas}}v_{\text{flow}}/y \sim 8.5 M_{\odot}\text{yr}^{-1}$, where $v_{\text{flow}} = v_s$ and $y = 15 \text{ kpc}$ are assumed. For well-known bright starburst galaxies, NGC 253 and M 82, the rates are $\dot{M}_{\text{flow}} = 5.8(v_{\text{flow}}/1000 \text{ kms}^{-1})(y/6.35 \text{ kpc})^{-1} M_{\odot}\text{yr}^{-1}$ (Strickland et al. 2002) and $12.9(v_{\text{flow}}/600 \text{ kms}^{-1})(y/6 \text{ kpc}) M_{\odot}\text{yr}^{-1}$ (Strickland et al. 1997), assuming the volume filling factor of the hot plasma to be 1 and a metal abundance of $Z=0.05$ solar. Thus, the mass-flow rate for HCG 80a is likely to be one of the largest among known starburst galaxies. Furthermore, like the cylindrical structure of the CO molecular gas observed in M 82 (Nakai et al. 1987), the outflow of cold matter undetectable in X-rays may raise the \dot{M}_{flow} value significantly if it exists. For example, if the total mass flow is ten-times larger than that estimated from the X-ray observation only, $t_{\text{SF}} = 40 \text{ Myr}$ would result in a total mass loss of $\sim 4 \times 10^9 M_{\odot}$. This corresponds to about 10% of the total galaxy mass inferred from the M/L_B ratio, $M \sim 4.7 \times 10^{10} M_{\odot}$.

In conclusion it is highly plausible that HCG 80a is a starburst galaxy that exhibits one of the most energetic outflows powered by starburst activity known in the universe.

4.3. Diffuse Hot Gas in HCG 80

We obtained a severe constraint on the intensity of the diffuse emission from the HCG 80 group region, $L_X < 6.3 \times 10^{40} \text{ erg s}^{-1}$, which is one of the lowest among the ROSAT groups of galaxies (figure 5). The flux sensitivity of the present *Chandra* observation is higher by a factor of about 25 than that of the previous ROSAT/PSPC observation (Ponman et al. 1996). Thus, it is clear that the current upper limit is lower by more than one order of

magnitude than that expected from the $\sigma - L_X$ relation. Compared to the X-ray luminosity of HCG 16 measured with XMM-Newton, $L_X = 5.0 \times 10^{40} h_{70}^{-2} \text{ erg s}^{-1}$ (Belsole et al. 2003), our upper limit is comparable to their result. If we further assume that the intragroup gas in HCG 80 is a 0.5 keV thermal plasma, distributed within a sphere of radius 50 kpc, the upper limits on the electron density and the total gas mass are estimated to be $n_e < 8.4 \times 10^{-4} \text{ cm}^{-3}$ and $M_{\text{IGM}} < 1.3 \times 10^{10} M_{\odot}$.

If we suppose that the HCG 80 group is a virialized system, and that the velocity dispersion properly measures the potential well, the total mass is $M_{\text{tot}} = 3\sigma_v^2 R/G \sim 3.4 \times 10^{12} M_{\odot}$, yielding a gas mass to the total mass ratio of < 0.004 . This unusually small value may be a consequence of the following possibilities: 1) HCG 80 is a chance alignment and not a real, physical system; 2) HCG 80 is a virializing, young system and the gas is yet to be heated to emit appreciable X-rays; or 3) the diffuse gas is expelled from HCG 80 by, for instance, violent activity of member galaxies.

Regarding the first possibility, the differences in the line-of-sight velocity relative to HCG 80a are $\Delta cz = +621, +587, +145 \text{ km s}^{-1}$ for HCG 80b, c, d, respectively (Arp 1997). They satisfy the criterion $\Delta cz < 1000 \text{ km s}^{-1}$ for the accordant system applied in Arp (1997). It is admittedly difficult to judge from the Δcz values alone whether galaxies are indeed concentrated compared to the field sample, since the velocity dispersion of the member galaxies, 309 km s^{-1} , corresponds to a comoving separation of 4.3 Mpc. The four members of HCG 80, however, are clustered within a circle of $r = 50.5 \text{ kpc}$ on the sky, yielding a cylindrical volume containing four galaxies of 0.07 Mpc^3 . This is only 1/15 of the mean occupied volume, $\sim 1 \text{ Mpc}^3$, of field galaxies brighter than HCG 80d ($B = 17$), based on the luminosity function in the SDSS b_j band (Blanton et al. 2001). This is supportive of a significant galaxy concentration in the HCG 80 group.

We further note that an exceptionally strong activity inferred in HCG 80a may be a result of galaxy interaction in the high-density environment. Coziol, Brinks, and Bravo-Alfaro (2004) quantified the level of activity (star formation or AGN) using a sample of 91 galaxies in the compact groups, and suggested an evolutionary sequence that groups at their early stage of evolution tend to be rich in late-type members with high activity levels, and show a smaller velocity dispersion. Since our results show that HCG 80 contains at least two active galaxies, and that the velocity dispersion of $\sigma_v = 309 \text{ km s}^{-1}$ is relatively small among their sample, HCG 80 is likely to be close to their configuration ‘‘type A’’, corresponding to a lower level of evolution. In addition, Verdes-Montenegro et al. (2001) showed that the groups richer in early type galaxies or more compact with larger velocity dispersion have a weak tendency to be more deficient in HI gas than expected from the optical luminosities, and proposed a scenario that the amount of HI gas would decrease further with evolution by tidal stripping and/or heating. Therefore, no significant HI deficiency in HCG 80 may also imply the lower level of evolution. In order to further confirm

the reality of the system and to constrain the physical properties, it is necessary to identify the distances of the HCG 80 galaxies, and also to search for evidence of interactions.

As pointed out by Mulchaey (2000), the hypothesis that the all spiral-only group is a mere chance alignment is unlikely given the existence of the our own spiral-only Local Group. We thus compare our result with the Local Group. Wang and McCray (1993) found the soft X-ray component with temperature 0.2 keV in the soft X-ray background, which could be due to a warm intragroup medium in the Local Group. Rasmussen, Kahn, and Paerels (2003) measured the absorption-line features towards three AGNs using the XMM-Newton/RGS deep spectroscopic data, whose redshift appear to be $z \sim 0$, and placed limits on the electron density, $n_e < 2 \times 10^{-4} \text{ cm}^{-3}$, the scale length of the absorber, $L > 140 \text{ kpc}$, and its mass, $M_{\text{IGM}} < 5 \times 10^{10} M_{\odot}$, in a collisional equilibrium approximation. Thus, the upper limit on the hot IGM in the HCG 80 group from the Chandra observation is similar to that of the Local Group, suggesting that the spiral-only groups may contain very tenuous IGM.

Another interpretation may be possible within the context of the preheating models for groups (e.g., Ponman et al. 1999). The model predicts that the energy input through galactic winds or outflows, powered by supernovae, should cause a more extended gas distribution, resulting in the gas density being too low to be detected in X-rays. Thus, the large halo emission discovered in HCG 80a and the low density of the intergalactic medium suggested from the analysis are not in conflict with the view of the preheating model. However, it is inconclusive because the non-detection of diffuse intragroup gas does not allow us to put any quantitative constraint on a connection between the outflowing gas and the intragroup gas. Additional follow-up observations will be meaningful to further clarify the role of late-type galaxies in the evolution of the IGM, probably at its early stage.

We are grateful to Y. Ishisaki and T. Oshima for their technical support and useful comments. N.O. acknowledges support from the Special Postdoctoral Researchers Program of RIKEN. U.M. is supported by a Research Fellowship for Young Scientists from JSPS. This research was supported in part by the Grant-in-Aid for Scientific Research of JSPS (14740133).

References

- Anders, E., & Grevesse, N. 1989, *Geochim. Cosmochim. Acta*, 53, 197
- Arp, H. 1997, *ApJ*, 474, 74
- Bahcall, N. A., Lubin, L. M., & Dorman, V. 1995, *ApJ*, 447, L81
- Belsole, E., Sauvageot, J.-L., Ponman, T. J., & Bourdin, H. 2003, *A&A*, 398, 1
- Blanton, M. R., et al. 2001, *AJ*, 121, 2358
- Coziol, R., Brinks, E., & Bravo-Alfaro, H. 2004, *AJ*, 128, 68
- Dickey, J. M., & Lockman, F. J. 1990, *ARA&A*, 28, 215

- Fukazawa, Y., Kawano, N., Ohta, A., & Mizusawa, H. 2002, PASJ, 54, 527
- Fukugita, M., Hogan, C. J., & Peebles, P. J. E. 1998, ApJ, 503, 518
- Green, P. J., et al. 1995, ApJ, 450, 51
- Heckman, T. M., Armus, L., & Miley, G. K. 1990, ApJS, 74, 833
- Helsdon, S. F., & Ponman, T. J. 2003, MNRAS, 340, 485
- Helsdon, S. F., Ponman, T. J., O'Sullivan, E., & Forbes, D. A. 2001, MNRAS, 325, 693
- Hickson, P. 1993, Astrophys. Lett. Comm., 29, 1
- Hickson, P. 1997, ARA&A, 35, 357
- Hickson, P., Kindl, E., & Auman, J. R. 1989, ApJS, 70, 687
- Kaastra, J. S. 1992, An X-Ray Spectral Code for Optically Thin Plasmas (Internal SRON-Leiden Report, updated version 2.0)
- Kennicutt, R. C. Jr. 1998, ARA&A, 36, 189
- Lehnert, M. D., Heckman, T. M., & Weaver, K. A. 1999, ApJ, 523, 575
- Liedahl, D. A., Osterheld, A. L., & Goldstein, W. H. 1995, ApJ, 438, L115
- Mewe, R., Gronenschild, E. H. B. M., & van den Oord, G. H. J. 1985, A&AS, 62, 197
- Mewe, R., Lemen, J. R., & van den Oord, G. H. J. 1986, A&AS, 65, 511
- Mulchaey, J. S. 2000, ARA&A, 38, 289
- Mulchaey, J. S., Davis, D. S., Mushotzky, R. F., & Burstein, D. 1996, ApJ, 456, 80
- Mulchaey, J. S., Davis, D. S., Mushotzky, R. F., & Burstein, D. 2003, ApJS, 145, 39
- Nakai, N., Hayashi, M., Handa, T., Sofue, Y., Hasegawa, T., & Sasaki, M. 1987, PASJ, 39, 685
- Nishiura, S., Shimada, M., Ohya, Y., Murayama, T., & Taniguchi, Y. 2000, AJ, 120, 1691
- Norman, C. A., & Ikeuchi, S. 1989, ApJ, 345, 372
- Oshima, T. 2003, PhD Thesis, The University of Tokyo
- Osmond, J. P. F., & Ponman, T. J. 2004, MNRAS, 350, 1511
- Ponman, T. J., Bourner, P. D. J., Ebeling, H., & Bohringer, H. 1996, MNRAS, 283, 690
- Ponman, T. J., Cannon, D. B., & Navarro, J. F. 1999, Nature, 397, 135
- Rasmussen, A., Kahn, S. M., & Paerels, F. 2003, in The IGM/Galaxy Connection: The Distribution of Baryons at $z=0$, ed. J. L. Rosenberg & M. E. Putman (Dordrecht: Kluwer Academic Publishers), 109
- Rubin, V. C., Ford, W. K. Jr., Thonnard, N., & Burstein, D. 1982, ApJ, 261, 439
- Sanders, D. B., & Mirabel, I. F. 1996, ARA&A, 34, 749
- Shimada, M., Ohya, Y., Nishiura, S., Murayama, T., & Taniguchi, Y. 2000, AJ, 119, 2664
- Strickland, D. K., Heckman, T. M., Colbert, E. J. M., Hoopes, C. G., & Weaver, K. A. 2004a, ApJS, 151, 193
- Strickland, D. K., Heckman, T. M., Colbert, E. J. M., Hoopes, C. G., & Weaver, K. A. 2004b, ApJ, 606, 829
- Strickland, D. K., Heckman, T. M., Weaver, K. A., Hoopes, C. G., & Dahlem, M. 2002, ApJ, 568, 689
- Strickland, D. K., Ponman, T. J., & Stevens, I. R. 1997, A&A, 320, 378
- Sulentic, J. W. 1997, ApJ, 482, 640
- Tully, R. B. 1987, ApJ, 323, 1
- Verdes-Montenegro, L., Yun, M. S., Williams, B. A., Huchtmeier, W. K., Del Olmo, A., & Perea, J. 2001, A&A, 377, 812
- Wang, Q. D., & McCray, R. 1993, ApJ, 409, L37